Probing heavy Higgs boson production and decay in the bestest little Higgs model at the LHC

E. Cruz-Albaro,[1,*] A. Gutiérrez-Rodríguez,[1,†] D. Espinosa-Gómez,[2,‡] T. Cisneros-Pérez,[3,§] and F. Ramírez-Zavaleta[2,‖]

[1]*Facultad de Física, Universidad Autónoma de Zacatecas, Apartado Postal C-580, 98060 Zacatecas, México*

[2]*Facultad de Ciencias Físico Matemáticas, Universidad Michoacana de San Nicolás de Hidalgo, Avenida Francisco, J. Mújica S/N, 58060, Morelia, Michoacán, México*

[3]*Unidad Académica de Ciencias Químicas, Universidad Autónoma de Zacatecas, Apartado Postal C-585, 98060 Zacatecas, México*

(Received 14 March 2024; accepted 28 May 2024; published 9 July 2024)

In the bestest little Higgs model (BLHM) scenario, we analyze the branching ratios and production cross section of the heavy Higgs boson H_0. The analysis is performed at the tree level and the one-loop level. In addition, we present results of the possible production of the heavy Higgs boson H_0 via gluon fusion for the center-of-mass energies and integrated luminosities of the LHC, HE-LHC, and HL-LHC. Our results show a very optimistic scenario for studying the H_0 scalar predicted by the BLHM and for the energies and luminosities of current and future hadron colliders.

DOI: 10.1103/PhysRevD.110.015013

I. INTRODUCTION

There are convincing theoretical arguments and a wide range of experimental facts that motivate the need for new physics beyond the Standard Model (SM), such as the hierarchy problem, the strong CP problem, the baryon asymmetry of the Universe, the existence of dark matter, the fine-tuning of the Higgs boson mass, the origin of fermionic families, etc. Most of the solutions to these problems require new interactions and new particles, such as supersymmetric partners, heavy Higgs bosons, dark photons, axions, right-handed neutrinos, and monopoles, among other things.

Many of the proposed new physics models contain an extended Higgs sector, among which the bestest little Higgs model (BLHM) [1–7] is one of the viable options because it provides an exciting way to address the hierarchy problem without resorting to fine-tuning. In addition, it solves some issues that are present in the great majority of the other little Higgs models [the littlest Higgs model [8], a littlest Higgs model with custodial $SU(2)$ symmetry [9], the little Higgs model [10], the little Higgs model and custodial $SU(2)$ [11], and the simplest little Higgs model [12]], such as the problem of dangerous singlets [13], a pathology where collective symmetry breaking does not suppress quadratically divergent corrections to the Higgs boson mass, and strong constraints from precision electroweak observables [14,15] in the gauge sector. Instead, the BLHM generates a viable Higgs quartic coupling where the real singlet σ is no longer a dangerous singlet; that is, it no longer develops a divergent tadpole from radiative corrections [1]. On the other hand, a custodial $SU(2)$ symmetry [16] and disassociation in the masses of the new quarks and heavy gauge bosons are implemented in the BLHM, thus avoiding the constraints from precision measurements.

The disassociation in the masses of the partners of fermions (T, B, T_5, T_6, $T^{2/3}$, $T^{5/3}$) and gauge bosons (Z', $W'^{\pm}$) is achieved by incorporating two independent symmetry-breaking scales f and F, with $F > f$. This leads to new quarks with masses proportional only to the f scale, while the new gauge bosons acquire masses proportional to the combination of the f and F scales. Since the new quarks are now lighter than the new gauge bosons, fine-tuning in the top sector and electroweak precision constraints in the gauge sector are avoided. In the scalar sector, neutral and charged physical scalar fields also arise: $h_0, H_0, A_0, \phi^0, \eta^0, H^{\pm}, \phi^{\pm}$, and $\eta^{\pm}$. The h_0 state is assumed to be light ($\approx$125 GeV), similar to the Higgs of the SM, while the masses of the rest of the scalars are allowed to vary.

*elicruzalbaro88@gmail.com
†alexgu@fisica.uaz.edu.mx
‡david.espinosa@umich.mx
§tzihue@gmail.com
‖feryuphy@yahoo.com.mx

In this paper, we explore the production of the heavy Higgs boson H_0 of the BLHM at current and future colliders such as the LHC and its upgrades, respectively. The discovery of any Higgs boson beyond the SM will be unequivocal evidence for the existence of an extended Higgs sector. Therefore, probing Higgs sectors of extended models through direct searches for new Higgs bosons at high-energy colliders or through modifications to SM-like Higgs couplings tested by precision measurements of the Higgs coupling take on a transcendental role [17]. The reason for this is that they open new routes to explore new physics effects.

Until now, direct and indirect searches for new physics at a weak scale have produced only unsuccessful results. However, new physics is expected to emerge at high masses, which means that it will be necessary to maximize the center-of-mass energy $\sqrt{s}$ of current colliders so that new heavy particles can be produced in collisions. This motivates the construction of more energetic colliders with higher luminosity $\mathcal{L}$. Therefore, the search for new physics beyond the SM remains a frontier in particle physics research.

The article is organized as follows. In Sec. II we review the BLHM. In Sec. III we present and study the tree-level and one-loop decays of the Higgs boson H_0. In Sec. IV we show the predictions of the BLHM in the production cross sections of the H_0 Higgs for the processes via gluon fusion. Finally, conclusions are presented in Sec. V.

II. REVIEW OF THE BLHM

The BLHM [1–7] is based on two independent nonlinear sigma models. With the first field Σ, the global $SO(6)_A \times SO(6)_B$ symmetry is broken to the diagonal group $SO(6)_V$ at the energy scale f, while with the second field Δ, the global $SU(2)_C \times SU(2)_D$ symmetry is broken to the diagonal subgroup $SU(2)$ to the scale F, with $F > f$. In the first stage, 15 pseudo-Nambu-Goldstone bosons are generated, which are parametrized as

$$\Sigma = e^{i\Pi/f} e^{2i\Pi_h/f} e^{i\Pi/f}, \tag{1}$$

where Π and Π_h are complex and antisymmetric matrices given by [1]

$$\Pi = \begin{pmatrix} i(\phi_a T_L^a + \eta_a T_R^a)_{4\times 4} & 0 & 0 \\ 0 & 0 & i\sigma/\sqrt{2} \\ 0 & -i\sigma/\sqrt{2} & 0 \end{pmatrix},$$
$$\Pi_h = \frac{i}{\sqrt{2}} \begin{pmatrix} 0_{4\times 4} & h_1 & h_2 \\ -h_1^T & 0 & 0 \\ -h_2^T & 0 & 0 \end{pmatrix}. \tag{2}$$

In Eq. (2), ϕ_a and η_a $(a = 1, 2, 3)$ are real triplets, h_1 and h_2 are **4**'s of $SO(4)$, and σ is a real singlet. For Higgs fields, their explicit representation is $h_i^T = (h_{i1}, h_{i2}, h_{i3}, h_{i4})$ [see Eqs. (16)–(23)], while $T_{L,R}^a$ denote the generators of the group $SO(6)$, which are provided in Refs. [1,13]. Regarding the second stage of symmetry breaking, the pseudo-Nambu-Goldstone bosons of the field Δ are parametrized as follows:

$$\Delta = F e^{2i\Pi_d/F}, \qquad \Pi_d = \chi_a \frac{\tau^a}{2} \quad (a = 1, 2, 3), \tag{3}$$

where χ_a represents the Nambu-Goldstone fields and the τ_a correspond to the Pauli matrices [1]. These latter are the generators of the SU(2) group.

A. Scalar sector

In order to generate a viable Higgs quartic coupling in the BLHM, we must explicitly break some of the symmetries under which Higgs fields transform nonlinearly. For this purpose, two operators are required, each of which explicitly breaks some of the global symmetries, but neither by itself would allow the Higgs to obtain a potential:

$$P_5 = \mathrm{diag}(0, 0, 0, 0, 1, 0), \qquad P_6 = \mathrm{diag}(0, 0, 0, 0, 0, 1). \tag{4}$$

In this way, the quartic potential is written as

$$\begin{aligned} V_q &= \frac{1}{4}\lambda_{65} f^4 \mathrm{Tr}(P_6 \Sigma P_5 \Sigma^T) + \frac{1}{4}\lambda_{56} f^4 \mathrm{Tr}(P_5 \Sigma P_6 \Sigma^T) \\ &= \frac{1}{4}\lambda_{65} f^4 (\Sigma_{65})^2 + \frac{1}{4}\lambda_{56} f^4 (\Sigma_{56})^2, \end{aligned} \tag{5}$$

where λ_{65} and λ_{56} are coefficients that must be nonzero to achieve collective symmetry breaking and generate a successful Higgs quartic coupling. From Eq. (5), the first term breaks $SO(6)_A \times SO(6)_B \to SO(5)_{A6} \times SO(5)_{B5}$, the $SO(5)_{A6}$ transformation protects h_1 from getting a potential, while $SO(5)_{B5}$ does the same for h_2. Similarly, the second term in Eq. (5) explicitly breaks $SO(6)_A \times SO(6)_B \to SO(5)_{A5} \times SO(5)_{B6}$. This symmetry allows the singlet σ to get a potential, while the other fields are protected. At this stage, if Eq. (1) is expanded as a power series in $1/f$ and substituted into Eq. (5), the following is obtained:

$$\begin{aligned} V_q = &\frac{\lambda_{65}}{2}\left(f\sigma - \frac{1}{\sqrt{2}} h_1^T h_2 + \cdots\right)^2 \\ &+ \frac{\lambda_{56}}{2}\left(f\sigma + \frac{1}{\sqrt{2}} h_1^T h_2 + \cdots\right)^2. \end{aligned} \tag{6}$$

In this expression, a mass term is generated for σ of the form $m_\sigma^2 = (\lambda_{65} + \lambda_{56}) f^2$. There are no mass terms generated for the Higgs fields.

While each of the terms in Eq. (6) seems to generate a Higgs quartic coupling, this quartic coupling can be eliminated by a redefinition of the σ field as $\sigma \to \pm\frac{h_1^T h_2}{\sqrt{2}f}$, where the upper and lower signs of the transformation correspond to the first and second operators in the mentioned equation. Collectively, however, the two terms of Eq. (6) yield a tree-level Higgs quartic coupling, which occurs after the scalar σ is integrated out [1,13,18]. Therefore,

$$V_q = \frac{\lambda_{56}\lambda_{65}}{\lambda_{56}+\lambda_{65}}\left(h_1^T h_2\right)^2 = \frac{1}{2}\lambda_0\left(h_1^T h_2\right)^2. \tag{7}$$

Equation (7) has the desired form of a collective quartic potential [1,13] and reaffirms that both terms of Eq. (6) are indeed necessary to generate a Higgs quartic coupling.

In the absence of gauge interactions, not all scalars obtain mass. Therefore, the following potential is added to generate them:

$$V_s = -\frac{f^2}{4}m_4^2\mathrm{Tr}\left(\Delta^\dagger M_{26}\Sigma M_{26}^\dagger + \Delta M_{26}\Sigma^\dagger M_{26}^\dagger\right) - \frac{f^2}{4}\left(m_5^2\Sigma_{55} + m_6^2\Sigma_{66}\right), \tag{8}$$

where m_4, m_5, and m_6 are mass terms and Σ_{55} and Σ_{66} represent the elements of the matrix Σ given in Eq. (1). On the other hand, M_{26} is a 2×6 matrix that contracts the $SU(2)$ indices of Δ with the SO(6) indices of Σ:

$$M_{26} = \frac{1}{\sqrt{2}}\begin{pmatrix} 0 & 0 & 1 & i & 0 & 0 \\ 1 & -i & 0 & 0 & 0 & 0 \end{pmatrix}. \tag{9}$$

Expanding the operator Δ [see Eq. (3)] as a power series in $1/F$ and substituting it into Eq. (8), we obtain

$$V_s = \frac{1}{2}(m_\phi^2\phi_a^2 + m_\eta^2\eta_a^2 + m_1^2 h_1^T h_1 + m_2^2 h_2^T h_2), \tag{10}$$

with

$$m_1^2 = \frac{1}{2}(m_4^2 + m_5^2), \tag{11}$$

$$m_2^2 = \frac{1}{2}(m_4^2 + m_6^2). \tag{12}$$

It is evident from Eq. (10) that the fields h_1, h_2, ϕ_a, and η_a get their masses.

In order to destabilize the origin and trigger electroweak symmetry breaking, the following potential is also introduced:

$$V_{B_\mu} = m_{56}^2 f^2\Sigma_{56} + m_{65}^2 f^2\Sigma_{65}, \tag{13}$$

where Σ_{56} and Σ_{65} denote the elements of the matrix Σ together with their mass parameters m_{56} and m_{65}, respectively. Finally, we have the full scalar potential of the BLHM,

$$V = V_q + V_s + V_{B_\mu}. \tag{14}$$

From this full potential, the potential for the Higgs doublet fields is obtained. For this task, one minimizes the potential of Eq. (14) with respect to the scalar σ and substitutes the resulting solution for σ back into Eq. (14). This results in the following Higgs potential [1,3,19]:

$$V_{\mathrm{Higgs}} = \frac{1}{2}m_1^2 h_1^T h_1 + \frac{1}{2}m_2^2 h_2^T h_2 - B_\mu h_1^T h_2 + \frac{\lambda_0}{2}\left(h_1^T h_2\right)^2, \tag{15}$$

where the components of the Higgs doublets $(h_1,\ h_2)$, B_μ, and λ_0 are explicitly expressed as

$$h_{11} = \cos\alpha h_0 - \sin\alpha H_0 + v\sin\beta, \tag{16}$$

$$h_{21} = \sin\alpha h_0 + \cos\alpha H_0 + v\cos\beta, \tag{17}$$

$$h_{12} = \cos\beta A_0, \tag{18}$$

$$h_{22} = \sin\beta A_0, \tag{19}$$

$$h_{13} = \frac{1}{\sqrt{2}}\left(\cos\beta(H^- + H^+)\right), \tag{20}$$

$$h_{14} = \frac{i}{\sqrt{2}}\left(\cos\beta(H^- - H^+)\right), \tag{21}$$

$$h_{23} = \frac{1}{\sqrt{2}}\left(\sin\beta(H^- + H^+)\right), \tag{22}$$

$$h_{24} = \frac{i}{\sqrt{2}}\left(\sin\beta(H^- - H^+)\right), \tag{23}$$

$$B_\mu = 2\frac{\lambda_{56}m_{65}^2 + \lambda_{65}m_{56}^2}{\lambda_{56}+\lambda_{65}}, \tag{24}$$

$$\lambda_0 = 2\frac{\lambda_{56}\lambda_{65}}{\lambda_{56}+\lambda_{65}}. \tag{25}$$

For the Higgs potential to reach a minimum, one must have $m_1 m_2 > 0$, while electroweak symmetry breaking requires that $B_\mu > m_1 m_2$.

Electroweak symmetry breaking in the BLHM is implemented when the Higgs doublets acquire their vacuum expectation values (VEVs), $\langle h_1\rangle^T = (v_1,0,0,0)$ and $\langle h_2\rangle^T = (v_2,0,0,0)$. These VEVs minimize the Higgs potential of

Eq. (15), thus generating the following relations:

$$v_1^2 = \frac{1}{\lambda_0}\frac{m_2}{m_1}(B_\mu - m_1 m_2), \tag{26}$$

$$v_2^2 = \frac{1}{\lambda_0}\frac{m_1}{m_2}(B_\mu - m_1 m_2). \tag{27}$$

The VEVs can be expressed in terms of the parameters v (the SM VEV) and $\tan\beta$ as follows:

$$v^2 \equiv v_1^2 + v_2^2 = \frac{1}{\lambda_0}\left(\frac{m_1^2 + m_2^2}{m_1 m_2}\right)(B_\mu - m_1 m_2) \simeq (246\ \mathrm{GeV})^2, \tag{28}$$

$$\tan\beta = \frac{v_1}{v_2} = \frac{m_2}{m_1}. \tag{29}$$

After electroweak symmetry breaking, the scalar sector of the BLHM generates several massive states: two physical scalar fields ($H^\pm$) and three neutral physical scalar fields (h_0, H_0, A_0). The lightest state, h_0, is identified as the Higgs boson of the SM. On the other hand, the four parameters in the Higgs potential m_1, m_2, B_μ, and λ_0 can be replaced by another more phenomenologically accessible set [3], that is, the masses of the states h_0 and A_0, the angle β, and the VEV v:

$$1 < \tan\beta < \sqrt{\frac{2 + 2\sqrt{\left(1 - \frac{m_{h_0}^2}{m_{A_0}^2}\right)\left(1 - \frac{m_{h_0}^2}{4\pi v^2}\right)}}{\frac{m_{h_0}^2}{m_{A_0}^2}\left(1 + \frac{m_{A_0}^2 - m_{h_0}^2}{4\pi v^2}\right)}} - 1, \tag{30}$$

$$B_\mu = \frac{1}{2}(\lambda_0 v^2 + m_{A_0}^2)\sin 2\beta, \tag{31}$$

$$\lambda_0 = \frac{m_{h_0}^2}{v^2}\left(\frac{m_{h_0}^2 - m_{A_0}^2}{m_{h_0}^2 - m_{A_0}^2 \sin^2 2\beta}\right), \tag{32}$$

$$\tan\alpha = \frac{B_\mu \cot 2\beta + \sqrt{(B_\mu^2/\sin^2 2\beta) - 2\lambda_0 B_\mu v^2 \sin 2\beta + \lambda_0^2 v^4 \sin^2 2\beta}}{B_\mu - \lambda_0 v^2 \sin 2\beta}, \tag{33}$$

$$m_{H^\pm}^2 = m_{A_0}^2 = m_1^2 + m_2^2, \tag{34}$$

$$m_{H_0}^2 = \frac{B_\mu}{\sin 2\beta} + \sqrt{\frac{B_\mu^2}{\sin^2 2\beta} - 2\lambda_0 B_\mu v^2 \sin 2\beta + \lambda_0^2 v^4 \sin^2 2\beta}, \tag{35}$$

$$m_\sigma^2 = (\lambda_{56} + \lambda_{65}) f^2 = 2\lambda_0 f^2 \mathrm{K}_\sigma \quad \text{with} \quad 1 < K_\sigma < \frac{16\pi^2}{\lambda_0(8\pi - \lambda_0)}. \tag{36}$$

The variables λ_{56} and λ_{65} in Eq. (36) represent the coefficients of the quartic potential [1], both variables take values different from zero to achieve the collective breaking of the symmetry and generate a quartic coupling of the Higgs boson [1,3].

B. Gauge sector

The kinetic terms of the gauge fields in the BLHM are given as follows:

$$\mathcal{L} = \frac{f^2}{8}\mathrm{Tr}(D_\mu \Sigma^\dagger D^\mu \Sigma) + \frac{F^2}{4}\mathrm{Tr}(D_\mu \Delta^\dagger D^\mu \Delta), \tag{37}$$

where the covariant derivatives are given by

$$D_\mu \Sigma = \partial_\mu \Sigma + i g_A A_{1\mu}^a T_L^a \Sigma - i g_B \Sigma A_{2\mu}^a T_L^a + i g_Y B_\mu^3 \left(T_R^3 \Sigma - \Sigma T_R^3\right), \tag{38}$$

$$D_\mu \Delta = \partial_\mu \Delta + i g_A A_{1\mu}^a \frac{\tau^a}{2}\Delta - i g_B \Delta A_{2\mu}^a \frac{\tau^a}{2}. \tag{39}$$

In these expressions, T_L^a are the generators of the group $SO(6)_A$ corresponding to the subgroup $SU(2)_{LA}$, while T_R^3 represents the third component of the $SO(6)_B$ generators corresponding to the $SU(2)_{LB}$ subgroup; these matrices are provided in Ref. [1]. g_A and $A_{1\mu}^a$ denote the gauge coupling

and field associated with the gauge bosons of $SU(2)_{LA}$. g_B and $A^a_{2\mu}$ represent the gauge coupling and the field associated with $SU(2)_{LB}$, while g_Y and B^3_μ denote the hypercharge and the field. When Σ and Δ get their VEVs, the gauge fields $A^a_{1\mu}$ and $A^a_{2\mu}$ are mixed to form a massless triplet $A^a_{0\mu}$ and a massive triplet $A^a_{H\mu}$,

$$\begin{aligned} A^a_{0\mu} &= \cos\theta_g A^a_{1\mu} + \sin\theta_g A^a_{2\mu}, \\ A^a_{H\mu} &= \sin\theta_g A^a_{1\mu} - \cos\theta_g A^a_{2\mu}, \end{aligned} \tag{40}$$

with the mixing angle

$$s_g \equiv \sin\theta_g = \frac{g_A}{\sqrt{g_A^2+g_B^2}}, \qquad c_g \equiv \cos\theta_g = \frac{g_B}{\sqrt{g_A^2+g_B^2}}, \tag{41}$$

which are related to the electroweak gauge coupling g through

$$g = \frac{g_A g_B}{\sqrt{g_A^2+g_B^2}}. \tag{42}$$

On the other hand, the weak mixing angle is defined as

$$s_W \equiv \sin\theta_W = \frac{g_Y}{\sqrt{g^2+g_Y^2}}, \qquad c_W \equiv \cos\theta_W = \frac{g}{\sqrt{g^2+g_Y^2}}. \tag{43}$$

In the BLHM, the masses of the new gauge bosons (Z' y $W'^{\pm}$) are also generated:

$$m^2_{Z'} = m^2_{W'^{\pm}} + \frac{g^2 s_W^2 v^4}{16 c_W^2 (f^2+F^2)}\left(s_g^2 - c_g^2\right)^2, \tag{44}$$

$$m^2_{W'^{\pm}} = \frac{g^2}{4 c_g^2 s_g^2}(f^2+F^2) - m^2_{W^{\pm}}. \tag{45}$$

C. Yang-Mills sector

The gauge boson self-interactions arise from the following Lagrangian terms:

$$\mathcal{L} = F_{1\mu\nu}F_1^{\mu\nu} + F_{2\mu\nu}F_2^{\mu\nu}, \tag{46}$$

where $F^{\mu\nu}_{1,2}$ are given explicitly as

$$F_1^{\mu\nu} = \partial^\mu A_1^{\alpha\nu} - \partial^\nu A_1^{\alpha\mu} + g_A \sum_b \sum_c \epsilon^{abc} A_1^{b\mu} A_1^{c\nu}, \tag{47}$$

$$F_2^{\mu\nu} = \partial^\mu A_2^{\alpha\nu} - \partial^\nu A_2^{\alpha\mu} + g_B \sum_b \sum_c \epsilon^{abc} A_2^{b\mu} A_2^{c\nu}. \tag{48}$$

The indices a, b, and c run over the three gauge fields [20] and ϵ^{abc} is the antisymmetric tensor.

D. Fermion sector

In the BLHM, the fermionic sector is divided into two parts. First, the massive fermion sector is represented by the Lagrangian of Eq. (49). This sector includes the top and bottom quarks of the SM and a series of new quarks arranged in four multiplets: Q and Q', which transform under $SO(6)_A$, and U^c and U'^c_5, which transform under the group $SO(6)_B$. Second, in the sector of light fermions contained in Eq. (58), all the interactions of the remaining fermions of the SM with the exotic particles of the BLHM are generated.

For massive fermions, the Lagrangian that describes them is given by [1]

$$\begin{aligned} \mathcal{L}_t = {} & y_1 f Q^T S \Sigma S U^c + y_2 f Q'^T \Sigma U^c + y_3 f Q^T \Sigma U'^c_5 \\ & + y_b f q_3^T (-2iT_R^2 \Sigma) U_b^c + \text{H.c.}, \end{aligned} \tag{49}$$

where $S = \text{diag}(1,1,1,1,-1,-1)$. The explicit representations of the multiplets involved in Eq. (49) are arranged as follows:

$$\begin{aligned} Q^T = \frac{1}{\sqrt{2}}\big(& (-Q_{a_1} - Q_{b_2}), i(Q_{a_1} - Q_{b_2}), (Q_{a_2} - Q_{b_1}), \\ & i(Q_{a_2} - Q_{b_1}), Q_5, Q_6\big), \end{aligned} \tag{50}$$

$$Q'^T = \frac{1}{\sqrt{2}}\left(-Q'_{a_1}, iQ'_{a_1}, Q'_{a_2}, iQ'_{a_2}, 0, 0\right), \tag{51}$$

$$q_3^T = \frac{1}{\sqrt{2}}\left(-\bar{t}_L, i\bar{t}_L, \bar{b}_L, i\bar{b}_L, 0, 0\right), \tag{52}$$

$$\begin{aligned} U^{cT} = \frac{1}{\sqrt{2}}\big(& (-U^c_{b_1} - U^c_{a_2}), i(U^c_{b_1} - U^c_{a_2}), (U^c_{b_2} - U^c_{a_1}), \\ & i(U^c_{b_2} - U^c_{a_1}), U^c_5, U^c_6\big), \end{aligned} \tag{53}$$

$$U'^{cT} = (0,0,0,0,U'^c_5,0), \tag{54}$$

$$U_b^{cT} = (0,0,0,0,b^c,0). \tag{55}$$

For simplicity, the Yukawa couplings y_i $(i=1,2,3)$ are assumed to be real [1,2]. These Yukawa couplings can also be written in terms of the Yukawa coupling of the top quark in the following way:

$$y_t = \frac{m_t}{v\sin\beta} = \frac{3y_1y_2y_3}{\sqrt{(y_1^2+y_2^2)(y_1^2+y_3^2)}}. \tag{56}$$

From Eq. (56), it is clear that the top Yukawa coupling is related to the three Yukawa couplings of the model, which in turn are part of the fine-tuning measure in the BLHM [1,18], Ψ, defined as

$$\Psi = \frac{27f^2}{8\pi^2\lambda_0 v^2\cos^2\beta}\frac{|y_1|^2|y_2|^2|y_3|^2}{|y_2|^2-|y_3|^2}\log\left(\frac{|y_1|^2+|y_2|^2}{|y_1|^2+|y_3|^2}\right). \quad (57)$$

As for the light fermions, their Lagrangian is

$$\mathcal{L}_{\text{light}} = \sum_{i=1,2} y_u f q_i^T \Sigma u_i^c + \sum_{i=1,2} y_d f q_i^T(-2iT_R^2\Sigma)d_i^c + \sum_{i=1,2,3} y_e f l_i^T(-2iT_R^2\Sigma)e_i^c + \text{H.c.}, \quad (58)$$

with

$$q_i^T = \frac{1}{\sqrt{2}}(-\bar{u}_{iL}, i\bar{u}_{iL}, \bar{d}_{iL}, i\bar{d}_{iL}, 0, 0), \quad (59)$$

$$l_i^T = \frac{1}{\sqrt{2}}(-\bar{\nu}_{iL}, i\bar{\nu}_{iL}, \bar{e}_{iL}, i\bar{e}_{iL}, 0, 0), \quad (60)$$

$$u_i^{cT} = (0,0,0,0,u_i^c,0), \quad (61)$$

$$d_i^{cT} = (0,0,0,0,d_i^c,0), \quad (62)$$

$$e_i^{cT} = (0,0,0,0,e_i^c,0). \quad (63)$$

With respect to the Yukawa couplings y_f $(f = u, d, e, b)$, these are associated with the masses of the fermions as

$$m_f^2 = y_f^2 v^2 \sin^2\beta\left(1-\frac{v^2}{3f^2}\right). \quad (64)$$

Since the top-quark loops provide the largest divergent corrections to the Higgs mass in the SM, the heavy-quark sector in the BLHM scenario is the most crucial for solving the hierarchy problem. The new heavy quarks arising in the BLHM are T, T_5, T_6, $T^{2/3}$, $T^{5/3}$, and B, whose associated masses are given as

$$m_T^2 = (y_1^2+y_2^2)f^2 + \frac{9v_1^2y_1^2y_2^2y_3^2}{(y_1^2+y_2^2)(y_2^2-y_3^2)}, \quad (65)$$

$$m_{T_5}^2 = (y_1^2+y_3^2)f^2 - \frac{9v_1^2y_1^2y_2^2y_3^2}{(y_1^2+y_3^2)(y_2^2-y_3^2)}, \quad (66)$$

$$m_{T_6}^2 = m_{T_b^{2/3}}^2 = m_{T_b^{5/3}}^2 = y_1^2 f^2, \quad (67)$$

$$m_B^2 = (y_1^2+y_2^2)f^2, \quad (68)$$

where $v_1 = v\sin\beta$ y $v_2 = v\cos\beta$. The mass terms for the new quarks, Eqs. (65)–(68), are calculated under the assumption that $y_2 \neq y_3$; otherwise, the masses of T and T_5 are degenerate at lowest order [2,18].

E. Currents sector

The Lagrangian that describes the interactions of fermions with the gauge bosons is [1,18]

$$\mathcal{L} = \bar{Q}\bar{\tau}^\mu D_\mu Q + \bar{Q}'\bar{\tau}^\mu D_\mu Q' - U^{c\dagger}\tau^\mu D_\mu U^c - U'^{c\dagger}\tau^\mu D_\mu U'^c - U_b^{c\dagger}\tau^\mu D_\mu U_b^c + \sum_{i=1,2} q_i^\dagger \tau^\mu D_\mu q_i + \sum_{i=1,2,3} l_i^\dagger \tau^\mu D_\mu l_i - \sum_{i=1,2,3} e_i^{c\dagger}\tau^\mu D_\mu e_i^c - \sum_{i=1,2} u_i^{c\dagger}\tau^\mu D_\mu u_i^c - \sum_{i=1,2} d_i^{c\dagger}\tau^\mu D_\mu d_i^c, \quad (69)$$

where τ^μ and $\bar{\tau}^\mu$ are defined according to Ref. [21]. On the other hand, the covariant derivatives are defined as follows:

$$D_\mu Q = \partial_\mu Q + \sum_a (ig_A A_{1\mu}^a T_L^a Q) + ig_Y B_{3\mu}(T_R^3 + T_X^+)Q, \quad (70)$$

$$D_\mu Q' = \partial_\mu Q' + \sum_a (ig_A A_{1\mu}^a T_L^a Q') + ig_Y B_{3\mu}\left(\frac{1}{6}\right)Q', \quad (71)$$

$$D_\mu U^c = \partial_\mu U^c + \sum_a (ig_B A_{2\mu}^a T_L^a U^c) + ig_Y B_{3\mu}(T_R^3 + T_X^-)U^c, \quad (72)$$

$$D_\mu U'^c = \partial_\mu U'^c + ig_Y B_{3\mu} T_X^- U'^c, \quad (73)$$

$$D_\mu U_b^c = \partial_\mu U_b^c + ig_Y B_{3\mu}\left(\frac{1}{3}\right)U_b^c, \quad (74)$$

$$D_\mu q_i = \partial_\mu q_i + \sum_a (ig_A A_{1\mu}^a T_L^a q_i) + ig_Y B_{3\mu}(T_R^3 + T_X^+)q_i, \quad (75)$$

$$D_\mu l_i = \partial_\mu l_i + \sum_a (ig_B A_{2\mu}^a T_L^a l_i) + ig_Y B_{3\mu} T_R^3 l_i, \quad (76)$$

$$D_\mu e_i^c = \partial_\mu e_i^c + ig_Y B_{3\mu} T_X^e e_i^c, \quad (77)$$

$$D_\mu u_i^c = \partial_\mu u_i^c + ig_Y B_{3\mu} T_X^- u_i^c, \quad (78)$$

$$D_\mu d_i^c = \partial_\mu d_i^c + ig_Y B_{3\mu} T_X^d d_i^c. \quad (79)$$

III. HEAVY HIGGS BOSON DECAYS IN THE BLHM

Recently, the first experimental evidence for the decay of the Higgs boson of the SM (h_0^{SM}) into a photon and a Z boson was presented, with a statistical significance of 3.4 standard deviations [22,23]. The result is derived from a combined analysis of the searches performed by the

ATLAS and CMS collaborations. In addition to this search channel, the diphoton decay of the SM Higgs is also a verified fact [24]. The $h_0^{\rm SM} \to \gamma\gamma, \gamma Z$ processes are essential particle physics as they are sensitive to possible contributions from physics beyond the SM and can even probe scenarios where the SM-like Higgs boson emerges. Although the $h_0^{\rm SM} \to \gamma\gamma, \gamma Z$ decay channels have small branching fractions, they provide a clean final-state topology, which can reconstruct the diphoton invariant mass and photon-$Z(\to ll, l = e \text{ or } \mu)$ invariant mass with high precision [22,24]. A new window to explore physics not described by the SM has opened with the discovery of the first fundamental scalar particle, $h_0^{\rm SM}$. Many of the extended models postulate the existence of heavy states. Linked to this, the search for additional scalar particles is being carried out by the ATLAS and CMS collaborations at the CERN LHC using data from increasingly energetic collisions. These facts motivate our study of the production of the H_0 Higgs of the BLHM at the LHC. For this purpose, we calculate the total decay width of the H_0 Higgs, where we consider direct search channels with SM final states. In the following, we describe the different decay modes of the Higgs boson H_0.

A. Two-body decays of the Higgs boson H_0 at tree level

In the BLHM, the Feynman diagrams representing the two-body decays of the H_0 Higgs at tree level are shown in Fig. 1. To calculate the partial decay widths of H_0, we use the Feynman rules for the interaction vertices provided in Refs. [5–7,25,26] and whose effective couplings we report in Appendix A.

The decay widths of $H_0 \to \bar{t}t, WW, ZZ, h_0h_0$ can be written as follows:

$$\Gamma(H_0 \to \bar{t}t) = \frac{N_c g_{H_0tt}^2 m_{H_0}}{8\pi}\left(1 - \frac{4m_t^2}{m_{H_0}^2}\right)^{3/2}, \tag{80}$$

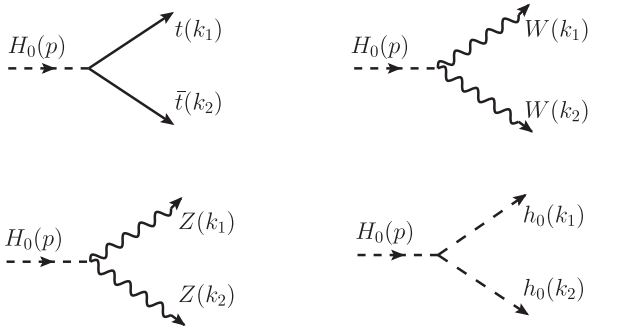

FIG. 1. Feynman diagrams corresponding to the two-body decays of the H_0 Higgs at tree level.

$$\Gamma(H_0 \to WW) = \frac{g_{H_0WW}^2 m_{H_0}^3}{64\pi m_W^4}\sqrt{1 - \frac{4m_W^2}{m_{H_0}^2}} \times \left(1 - \frac{4m_W^2}{m_{H_0}^2} + \frac{12m_W^4}{m_{H_0}^4}\right), \tag{81}$$

$$\Gamma(H_0 \to ZZ) = \frac{g_{H_0ZZ}^2 m_{H_0}^3}{128\pi m_Z^4}\sqrt{1 - \frac{4m_Z^2}{m_{H_0}^2}} \times \left(1 - \frac{4m_Z^2}{m_{H_0}^2} + \frac{12m_Z^4}{m_{H_0}^4}\right), \tag{82}$$

$$\Gamma(H_0 \to h_0h_0) = \frac{g_{H_0h_0h_0}^2}{32\pi m_{H_0}}\sqrt{1 - \frac{4m_{h_0}^2}{m_{H_0}^2}}, \tag{83}$$

where $N_c = 3$, is the color factor and $g_{H_0tt}, g_{H_0WW}, g_{H_0ZZ}$, and $g_{H_0h_0h_0}$ represent the couplings of the interaction vertices involved in the tree-level processes, which are given in Appendix A [5–7,25,26].

B. Three-body decays of the Higgs boson H_0 at tree level

Concerning the three-body decays of the H_0 Higgs, the Feynman diagrams that arise for these processes are shown in Fig. 2. The scalar particles and gauge bosons of the SM and the BLHM mediate these processes. The effective couplings for the interaction vertices are given in Appendix A [5–7,25]. We only provide the decay amplitudes because the expressions generated for the partial widths are quite lengthy. The analytical expressions for the decay widths of the H_0 Higgs decaying to three bodies can be calculated using the generic formula described in Eq. (84) [27,28],

$$\frac{d\Gamma(H_0 \to ABC)}{dx_a dx_b} = \frac{m_{H_0}}{256\pi^3}|\mathcal{M}(H_0 \to ABC)|^2. \tag{84}$$

It is worth mentioning that for some decay channels of the H_0 Higgs, specific interaction vertices ($Z'WW$, h_0WW', and h_0ZZ') cancel out. This happens because in the BLHM the gauge couplings g_A and g_B, associated with the gauge bosons $SU(2)_{LA}$ and $SU(2)_{LB}$, can be parametrized in a more phenomenological fashion in terms of a mixing angle θ_g, $\tan\theta_g = g_A/g_B$. For simplicity, it is assumed that $\tan\theta_g = 1$ [6,18], which implies that the gauge couplings g_A and g_B are equal, i.e., $\sin\theta_g = \cos\theta_g$ ($s_g = c_g$). This fact leads to no contribution from specific decay amplitudes. The only contributing amplitudes are

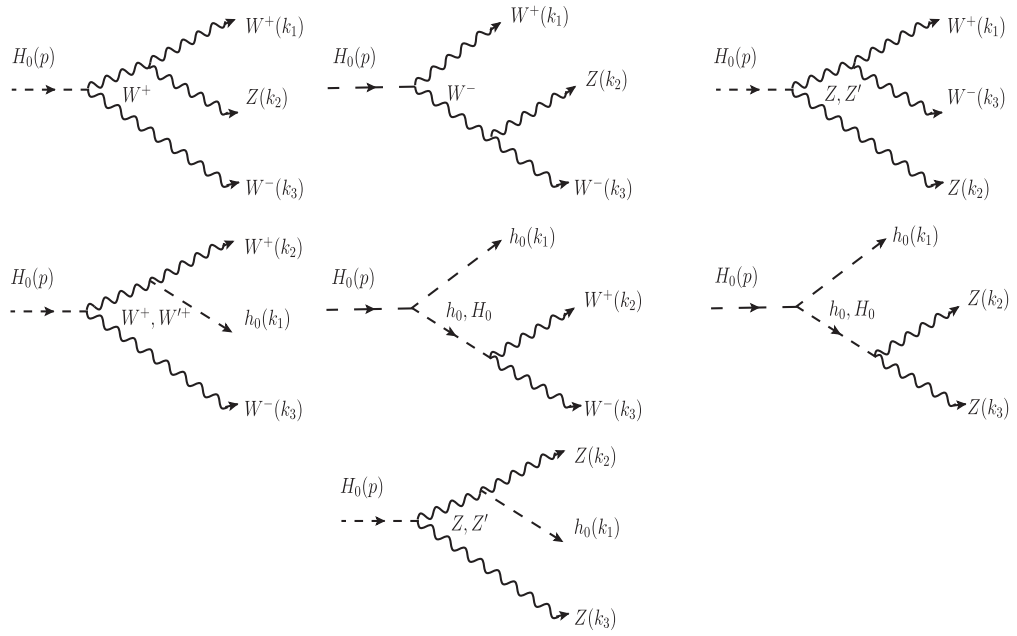

FIG. 2. Feynman diagrams corresponding to the three-body decays of the H_0 Higgs at tree level.

given in Eqs. (85)–(87):

$$\mathcal{M}(H_0 \to WZZ) = i g_{WWZ}\Bigg[-\frac{g_{H_0WW}}{(k_1+k_2)^2-m_W^2}\Bigg(\big(k_1^\mu+2k_2^\mu\big)g^{\alpha\nu}-(2k_1^\nu+k_2^\nu)g^{\alpha\mu}+\Bigg(-2k_2^\alpha+\frac{m_Z^2}{m_W^2}(k_1^\alpha+k_2^\alpha)\Bigg)g^{\mu\nu}$$
$$+\frac{(k_1^\alpha+k_2^\alpha)(k_1^\mu k_1^\nu-k_2^\mu k_2^\nu)}{m_W^2}\Bigg)+\frac{g_{H_0WW}}{(k_2+k_3)^2-m_W^2}\Bigg((2k_2^\alpha+k_3^\alpha)g^{\mu\nu}+\frac{(k_3^\alpha k_3^\nu-k_2^\alpha k_2^\nu)(k_2^\mu+k_3^\mu)}{m_W^2}$$
$$+\Bigg(-2k_2^\mu+\frac{m_Z^2}{m_W^2}(k_2^\mu+k_3^\mu)\Bigg)g^{\alpha\nu}-(k_2^\nu+2k_3^\nu)g^{\alpha\mu}\Bigg)+\frac{g_{H_0ZZ}}{(k_1+k_3)^2-m_Z^2}\Bigg(-(k_1^\mu+2k_3^\mu)g^{\alpha\nu}$$
$$-(k_1^\nu-k_3^\nu)g^{\alpha\mu}+(2k_1^\alpha+k_3^\alpha)g^{\mu\nu}+\frac{(k_3^\alpha k_3^\mu-k_1^\alpha k_1^\mu)(k_1^\nu+k_3^\nu)}{m_Z^2}\Bigg)\Bigg]\epsilon_\mu^*(k_1)\epsilon_\nu^*(k_2)\epsilon_\alpha^*(k_3), \tag{85}$$

$$\mathcal{M}(H_0 \to h_0WW) = i\Bigg[\Bigg(\frac{g_{h_0H_0H_0}g_{H_0WW}}{(k_2+k_3)^2-m_{H_0}^2}+\frac{g_{H_0h_0h_0}g_{h_0WW}}{(k_2+k_3)^2-m_{h_0}^2}+\frac{g_{H_0WW}g_{h_0WW}}{(k_1+k_2)^2-m_W^2}\Bigg)g^{\mu\nu}$$
$$-\frac{g_{h_0WW}g_{H_0WW}(k_1^\mu+k_2^\mu)(k_1^\nu+k_2^\nu)}{m_W^2((k_1+k_2)^2-m_W^2)}\Bigg]\epsilon_\mu^*(k_2)\epsilon_\nu^*(k_3), \tag{86}$$

$$\mathcal{M}(H_0 \to h_0ZZ) = i\Bigg[\Bigg(\frac{g_{h_0H_0H_0}g_{H_0ZZ}}{(k_2+k_3)^2-m_{H_0}^2}+\frac{g_{H_0h_0h_0}g_{h_0ZZ}}{(k_2+k_3)^2-m_{h_0}^2}+\frac{g_{H_0ZZ}g_{h_0ZZ}}{(k_1+k_2)^2-m_Z^2}\Bigg)g^{\mu\nu}$$
$$-\frac{g_{h_0ZZ}g_{H_0ZZ}(k_1^\mu+k_2^\mu)(k_1^\nu+k_2^\nu)}{m_Z^2((k_1+k_2)^2-m_Z^2)}\Bigg]\epsilon_\mu^*(k_2)\epsilon_\nu^*(k_3). \tag{87}$$

C. Two-body decays of the Higgs boson H_0 at one-loop level

This subsection determines the amplitudes and partial decay widths of the H_0 Higgs at the one-loop level. In Fig. 3, we show the Feynman diagrams associated with the $H_0 \to \gamma\gamma, \gamma Z, gg$ decays which are mediated by fermions $(t; T; T^{2/3}; T_5; T_6)$ and gauge bosons $(W^\pm; W'^\pm)$ of the SM and BLHM. These H_0 decays are absent at the tree level in the BLHM. However, they arise at the one-loop level, which is of great interest since they not only help to examine

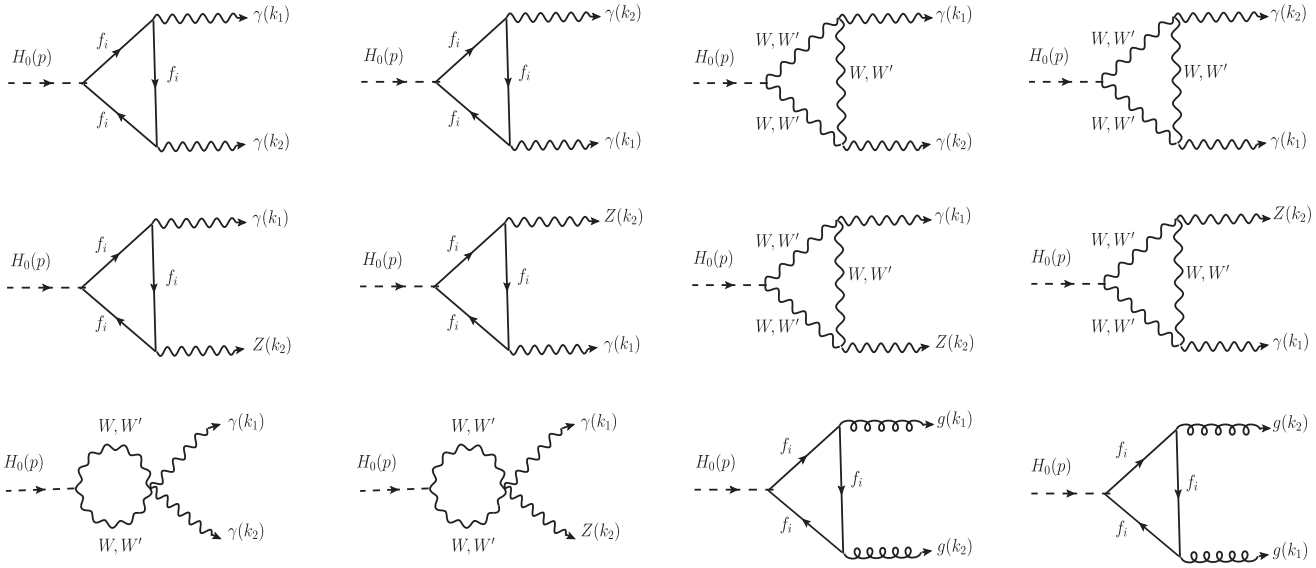

FIG. 3. Feynman diagrams corresponding to the two-body decays of the H_0 Higgs at one-loop level. The notation f_i represents the $t, T, T^{2/3}, T_5, T_6$ quarks.

higher-order corrections to the theory but also provide information about possible contributions from new particles circulating in the loop.

In the following, all calculations at the one-loop level are carried out using the unitary gauge and the Passarino-Veltman reduction scheme [29]. In this way, we find that the total amplitude for the first decay $H_0 \to \gamma\gamma$ can be written as

$$\mathcal{M}(H_0 \to \gamma\gamma) = \left(A_f^{\gamma\gamma} + A_W^{\gamma\gamma} + A_{W'}^{\gamma\gamma}\right)(k_1^\nu k_2^\mu - k_1 \cdot k_2 g^{\mu\nu})\epsilon_\mu^*(k_1)\epsilon_\nu^*(k_2), \tag{88}$$

where the form factors $A_f^{\gamma\gamma}$, $A_W^{\gamma\gamma}$, $A_{W'}^{\gamma\gamma}$ are defined as follows:

$$A_f^{\gamma\gamma} = \frac{N_c}{2\pi^2 m_{H_0}^2} \sum_{f=t,T,T_5,T_6,T^{2/3}} g_{H_0 ff}(g_{Aff})^2 m_f Q_f \left(2 - (m_{H_0}^2 - 4m_f^2) C_0(m_{H_0}^2, 0, 0, m_f^2, m_f^2, m_f^2)\right), \tag{89}$$

$$A_W^{\gamma\gamma} = \frac{g_{H_0 WW}(g_{WWA})^2}{8\pi^2 m_{H_0}^2}\left(6\left(m_{H_0}^2 - 2m_W^2\right)C_0\left(m_{H_0}^2, 0, 0, m_W^2, m_W^2, m_W^2\right) - \frac{m_{H_0}^2}{m_W^2} - 6\right), \tag{90}$$

$$A_{W'}^{\gamma\gamma} = \frac{g_{H_0 W'W'}(g_{W'W'A})^2}{8\pi^2 m_{H_0}^2}\left(6\left(m_{H_0}^2 - 2m_{W'}^2\right)C_0\left(m_{H_0}^2, 0, 0, m_{W'}^2, m_{W'}^2, m_{W'}^2\right) - \frac{m_{H_0}^2}{m_{W'}^2} - 6\right). \tag{91}$$

The labels f and W (W') of the form factors $A_f^{\gamma\gamma}$ and $A_W^{\gamma\gamma}$ ($A_{W'}^{\gamma\gamma}$), respectively, represent the contributions generated due to the quarks and gauge bosons circulating in the loop of the diphoton decay of H_0 Higgs. On the other hand, $C_0(m_{H_0}^2, 0, 0, m_f^2, m_f^2, m_f^2)$, $C_0(m_{H_0}^2, 0, 0, m_W^2, m_W^2, m_W^2)$, and $C_0(m_{H_0}^2, 0, 0, m_{W'}^2, m_{W'}^2, m_{W'}^2)$ denote the scalar functions of the Passarino-Veltman reduction scheme.

Using Eq. (88), we find that the decay width for the $H_0 \to \gamma\gamma$ process is

$$\Gamma(H_0 \to \gamma\gamma) = \frac{1}{64\pi}\left|A_f^{\gamma\gamma} + A_W^{\gamma\gamma} + A_{W'}^{\gamma\gamma}\right|^2 m_{H_0}^3. \tag{92}$$

The one-loop decay amplitude for the second process $H_0 \to \gamma Z$ is

$$\mathcal{M}(H_0 \to \gamma Z) = \left(A_f^{\gamma Z} + A_W^{\gamma Z} + A_{W'}^{\gamma Z}\right)\left(k_1^\nu k_2^\mu - k_1.k_2 g^{\mu\nu}\right)\epsilon_\mu^*(k_1)\epsilon_\nu^*(k_2), \tag{93}$$

with

$$A_f^{\gamma Z} = \frac{N_c}{2\pi^2(m_{H_0}^2 - m_Z^2)^2} \sum_{f=t,T,T_5,T_6,T^{2/3}} m_f Q_f \big[g_{H_0 ff} g_{Aff} g_{Zff} \big(\big(m_{H_0}^2 - m_Z^2\big)\big(m_Z^2 + 4m_f^2 - m_{H_0}^2\big) \times C_0\big(m_{H_0}^2, 0, 0, m_f^2, m_f^2, m_f^2\big) + 2\big) - 2m_Z^2 \big(B_0\big(m_Z^2, m_f^2, m_f^2\big) - B_0\big(m_{H_0}^2, m_f^2, m_f^2\big)\big)\big], \tag{94}$$

$$A_W^{\gamma Z} = \frac{g_{H_0 WW} g_{WWA} g_{WWZ}}{16\pi^2 t_W^4 (1 - t_Z^2) m_{H_0}^2} \big[\big(12t_W^4 - 2t_W^2(t_Z^2 - 1) - t_Z^2\big)\big(t_Z^2(B_0(m_{H_0}^2, m_W^2, m_W^2) - B_0(m_Z^2, m_W^2, m_W^2) - 1) + 1\big) - 2t_W^2(t_Z^2 - 1)(12t_W^4 + 6t_W^2(t_Z^2 - 1) - t_Z^2(2t_Z^2 - 1)) m_{H_0}^2 C_0(m_{H_0}^2, m_Z^2, 0, m_W^2, m_W^2, m_W^2)\big], \tag{95}$$

and

$$A_{W'}^{\gamma Z} = \frac{g_{H_0 W'W'} g_{W'W'A} g_{W'W'Z}}{16\pi^2 t_{W'}^4 (1 - t_Z^2) m_{H_0}^2} \big[\big(12t_{W'}^4 - 2t_{W'}^2(t_Z^2 - 1) - t_Z^2\big)\big(t_Z^2(B_0(m_{H_0}^2, m_{W'}^2, m_{W'}^2) - B_0(m_Z^2, m_{W'}^2, m_{W'}^2) - 1) + 1\big) - 2t_{W'}^2(t_Z^2 - 1)\big(12t_{W'}^4 + 6t_{W'}^2(t_Z^2 - 1) - t_Z^2(2t_Z^2 - 1)\big) m_{H_0}^2 C_0\big(m_{H_0}^2, m_Z^2, 0, m_{W'}^2, m_{W'}^2, m_{W'}^2\big)\big], \tag{96}$$

where $t_W = \frac{m_W}{m_{H_0}}$, $t_Z = \frac{m_Z}{m_{H_0}}$ and $t_{W'} = \frac{m_{W'}}{m_{H_0}}$. It is worth mentioning that the form factors $A_f^{\gamma Z}$, $A_W^{\gamma Z}$, and $A_{W'}^{\gamma Z}$ provide finite results, i.e., these are free of ultraviolet divergences. For the $H_0 \to \gamma Z$ decay, their corresponding decay width is

$$\Gamma(H_0 \to \gamma Z) = \frac{1}{32\pi m_{H_0}^3} \big| A_f^{\gamma Z} + A_W^{\gamma Z} + A_{W'}^{\gamma Z} \big|^2 \big(m_{H_0}^2 - m_Z^2\big)^3. \tag{97}$$

Finally, the decay amplitude of the process $H_0 \to gg$ is as follows:

$$\mathcal{M}(H_0 \to gg) = A^{gg}(k_1^\nu k_2^\mu - k_1.k_2 g^{\mu\nu}) \epsilon_\mu^{*a}(k_1) \epsilon_\nu^{*b}(k_2) \delta_{ab}, \tag{98}$$

where

$$A^{gg} = \frac{N_c}{4\pi^2 m_{H_0}^2} \sum_{f=t,T,T_5,T_6,T^{2/3}} g_{H_0 ff} (g_{g_s ff})^2 m_f \times \big(2 - \big(m_{H_0}^2 - 4m_f^2\big) C_0\big(m_{H_0}^2, 0, 0, m_f^2, m_f^2, m_f^2\big)\big). \tag{99}$$

The corresponding decay width for the $H_0 \to gg$ process is given by

$$\Gamma(H_0 \to gg) = \frac{1}{8\pi} |A^{gg}|^2 m_{H_0}^3. \tag{100}$$

IV. NUMERICAL RESULTS

To carry out our numerical analysis of the Higgs production H_0 in the context of the BLHM, we briefly review some free parameters of the model of interest and provide in Table I the values assigned to these parameters.

A. A measure of fine-tuning in the BLHM

As discussed in Refs. [2,5,7], the three Yukawa couplings, y_1, y_2, and y_3 generate two study scenarios in the BLHM, which arise because in the region where $y_2 \approx y_3$ the masses of T and T_5 are degenerate to the lowest order. Consequently, different diagonalization schemes are required for the fermion mass matrix when $y_2 \approx y_3$ versus $|y_2 - y_3| > 0$. The two study scenarios to which we refer are:

(1) Scenario a: $(y_2 < y_3)$, $y_1 = 0.61$, $y_2 = 0.35$ and $y_3 = 0.84$ [5–7],
(2) Scenario b: $(y_2 > y_3)$, $y_1 = 0.61$, $y_2 = 0.84$ and $y_3 = 0.35$ [5–7].

Our choice in the values of y_i are motivated by the perturbativity requirements [30] and the fine-tuning measure [1,2]. Using numerical methods, from Eq. (56), we randomize perturbative values of the Yukawa couplings y_i by fixing y_t through experimental measurements of the top-quark mass [31] and the Higgs boson mass

TABLE I. Values assigned to the parameters involved in our numerical analysis in the BLHM.

Parameter	Value	Reference
m_{h_0}	125.25 GeV	[31]
m_{A_0}	1000 GeV	[32,33]
$\tan\beta$	3	[5–7]
m_{H_0}	1015 GeV	[32]
$g_A = g_B$	$\sqrt{2}g$	[5–7]
f	$[1000, 3000]$ GeV	[1,3,5–7]
F	$[3000, 6000]$ GeV	[1,3,5–7]

($m_{h_0} = 125.25$ GeV [31]), and an appropriate choice of the free parameters m_{A_0} and $\tan\beta$ [see Eqs. (30) and (56)], as discussed below.

1. Pseudoscalar mass A_0

This parameter is fixed around 1000 GeV, which is consistent with the current search results for new scalar bosons [32,33]. Data recorded by the ATLAS experiment at the LHC, corresponding to an integrated luminosity of 139 fb^{-1} from pp collisions at a center-of-mass energy of 13 TeV, were used to search for a heavy Higgs boson, A_0, decaying into ZH_0, where H_0 denotes another Higgs boson with mass $m_{H_0} > 125$ GeV.

2. Ratio of the VEVs of the two Higgs doublets, $\tan\beta$

A lower bound emerges for $\tan\beta$ when examining the radiative corrections to m_1 and m_2 in the BLHM, which suggests that $\tan\beta > 1$ [1]. On the other hand, the authors of Ref. [3] set an upper bound to $\tan\beta$ that arises due to perturbativity requirements on the parameter λ_0. Thus, the range of values that the parameter $\tan\beta$ could acquire is set according to Eq. (30). Using this equation, for $m_{A_0} = 1000$ GeV, it is obtained that $1 < \tan\beta < 10.45$. Consistently, in this paper we chose $\tan\beta = 3$ [5–7] to carry out our numerical analysis of the production of the Higgs boson H_0.

In this way, scenarios a and b mentioned above offer realistic values of the Yukawa couplings as they satisfy the perturbativity requirements and minimize the fine-tuning constraints as the energy scale f takes on values close to 3000 GeV. Hence, from Eq. (57) we determine the size of the fine-tuning as the scale of the new physics f takes certain values in the range of 1 to 3 TeV. In Table II, we show a measure of the fine-tuning when the energy scale f takes on values such as 1.0, 1.5, 2.0, 2.5, and 3.0 TeV. According to the numerical values listed in Table II, the size of the fine-tuning when $f = 1.0$ TeV is $\Psi = 0.54$, which indicates that there is no fine-tuning in the BLHM [1,18]. The absence of fine-tuning prevails up to $\Psi = 2.2$, i.e., for values of the energy scale f close to 2 TeV. The fine-tuning starts to become significant for $f > 2.1$ TeV.

In the following numerical analysis, our results are generated only for scenario a, proposed above. Scenario b provides nearly identical results. As a summary, we provide in Table I the values assigned to the parameters involved in our calculation.

TABLE II. Measure of the fine-tuning in the BLHM for some values of the f scale.

f [TeV]	Ψ
1.0	0.54
1.5	1.21
2.0	2.16
2.5	3.37
3.0	4.85

Due to the characteristics of the BLHM, this is based on two independent global symmetries that break into diagonal subgroups at different energy scales, f and F. These scales represent the scales of the new physics. Therefore, it is convenient to analyze the H_0 production cross section as a function of the energy scales f and F since the masses of the particles circulating in the loop of the $H_0 \to \gamma\gamma, \gamma Z, gg$ processes depend on the scales f and F. On the other hand, one-loop decays of H_0 into $\gamma\gamma$, γZ, and gg will be helpful to test the consistency of the current parameter space of the BLHM.

For the purposes mentioned above, we begin by presenting a numerical analysis of the decay widths for the $H_0 \to tt, h_0h_0, gg, WW, ZZ, h_0WW, h_0ZZ, WWZ, \gamma\gamma, \gamma Z$ processes. In this way, in Fig. 4 we show the behavior of $\Gamma(H_0 \to X)$ versus f and $\Gamma(H_0 \to X)$ versus F, where $\Gamma(H_0 \to X)$ denotes the partial decay width of the H_0 Higgs. From the first plot [see Fig. 4(a)], we can appreciate that the dominant and subdominant contributions to the decay width of H_0 (Γ_{H_0}) over the whole analysis interval of scale f come from the tree-level decays of H_0 into $\bar{t}t$ and h_0h_0, respectively. The numerical contributions of these decays are $\Gamma(H_0 \to \bar{t}t) \sim 10^0$ GeV and $\Gamma(H_0 \to h_0h_0) \sim 10^{-1}$ GeV. For this last contribution, the decay channels $H_0 \to gg$ and $H_0 \to WW$ also contribute with the same order of magnitude, although they are slightly smaller than $\Gamma(H_0 \to h_0h_0)$. Notice that the $H_0 \to gg$ process is a one-loop decay. Other decay modes that contribute at lower order but contribute significantly to Γ_{H_0} are the $H_0 \to ZZ, h_0WW, h_0ZZ, WWZ$ decays, whose associated decay widths are of 10^{-2}–10^{-3} GeV when $f \in [1000, 3000]$ GeV, which are all tree-level decays. For the remaining one-loop decays, we find that the $H_0 \to \gamma\gamma, \gamma Z$ decays provide suppressed contributions to the decay width of the H_0 Higgs: $\Gamma(H_0 \to \gamma\gamma) \sim \Gamma(H_0 \to \gamma Z) \sim 10^{-4}$ GeV. For a better numerical appreciation of the changes of the different partial decay widths of the H_0 Higgs as the f scale takes values from 1000 to 3000 GeV, in Appendix B we show some of the values of $\Gamma(H_0 \to X)$ when f takes values such as 1000, 2000, and 3000 GeV. Regarding the second plot [see Fig. 4(b)], which examines the dependence of $\Gamma(H_0 \to X)$ on the energy scale F, we observe that the largest contributions to Γ_{H_0} are again generated by the $H_0 \to \bar{t}t, h_0h_0$ decays: $\Gamma(H_0 \to \bar{t}t) \sim 10^0$ GeV and $\Gamma(H_0 \to h_0h_0) \sim 10^{-1}$ GeV for the interval of $F = [3000, 6000]$ GeV. The processes $H_0 \to gg, WW$ and $H_0 \to ZZ, h_0WW, h_0ZZ$ also contribute considerably to the decay width of H_0; for these decays, we find that the corresponding numerical estimates are $\Gamma(H_0 \to gg) \sim \Gamma(H_0 \to WW) \sim 10^{-1}$ GeV and $\Gamma(H_0 \to ZZ) \sim \Gamma(H_0 \to h_0WW) \sim \Gamma(H_0 \to h_0ZZ) \sim 10^{-2}$ GeV. Finally, the curves that provide the most suppressed contributions compared to

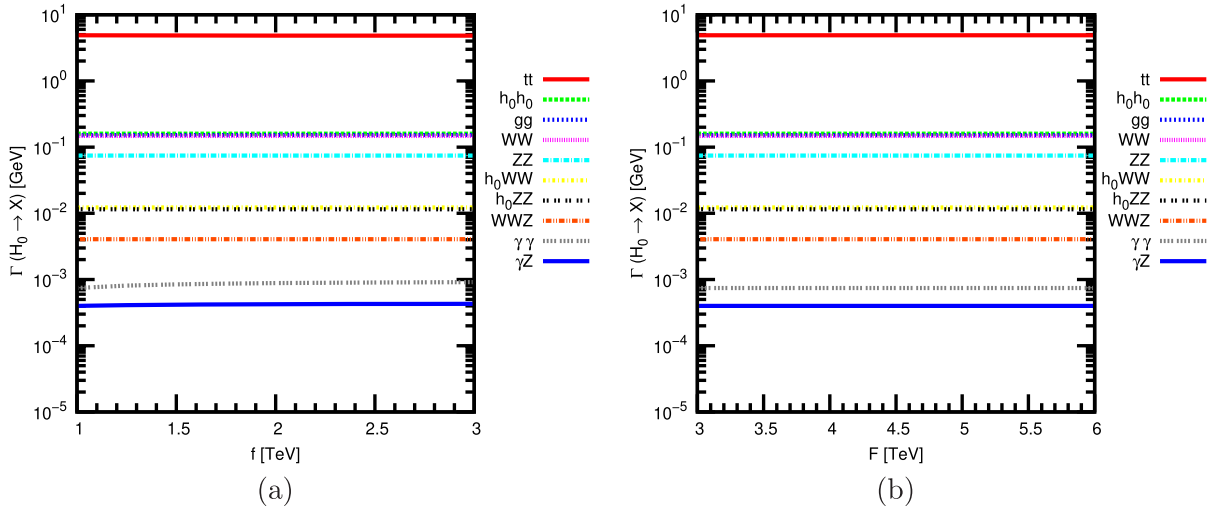

FIG. 4. Decay widths for the $H_0 \to X$ processes where $X = tt, h_0h_0, gg, WW, ZZ, h_0WW, h_0ZZ, WWZ, \gamma\gamma, \gamma Z$. (a) $\Gamma(H_0 \to X)$ as a function of the f energy scale (with the fixed value of $F = 4000$ GeV). (b) $\Gamma(H_0 \to X)$ as a function of the F energy scale (with the fixed value of $f = 1000$ GeV).

the main contribution come from the $H_0 \to WWZ$ and $H_0 \to \gamma\gamma, \gamma Z$ decays; their predicted numerical magnitudes are 3 and 4 orders of magnitude smaller than $\Gamma(H_0 \to \bar{t}t)$, while the F scale acquires values in the range of 3000 to 6000 GeV. We also report in Appendix B the numerical values of $\Gamma(H_0 \to X)$ for a single value of the energy scale F, $F = 3000$ GeV. This is because the values that $\Gamma(H_0 \to X)$ acquires over the whole range set for F remain almost a constant, and the numerical sensitivity is reflected up to several orders of magnitude lower than that reported in the corresponding table in Appendix B. In summary, the numerical evaluation tells us that the tree-level decay channel $H_0 \to \bar{t}t$ provides the most significant contribution to the H_0 decay width. In contrast, the $H_0 \to \gamma Z$ decay at the one-loop level generates the most minor contribution. On the other hand, we find that $\Gamma(H_0 \to X)$ shows a greater sensitivity to the f scale compared to another scale of the new physics, F.

We also calculate the branching ratios of the Higgs boson H_0 as functions of the energy scale f and F, as shown in Fig. 5. The plots are obtained considering the total decay width of the H_0 Higgs, which contains the following decay modes: $\bar{t}t, WW, ZZ, h_0h_0, h_0WW, h_0ZZ, WWZ, \gamma\gamma, \gamma Z, gg$. From Fig. 5(a), we can see the curves that represent the estimates of the branching ratios versus the f scale when it takes values from 1000 to 3000 GeV. The $H_0 \to \bar{t}t$ decay yields the highest contribution; its associated branching ratio is $\mathrm{Br}(H_0 \to \bar{t}t) \sim 10^{-1}$. On the opposite side, we find

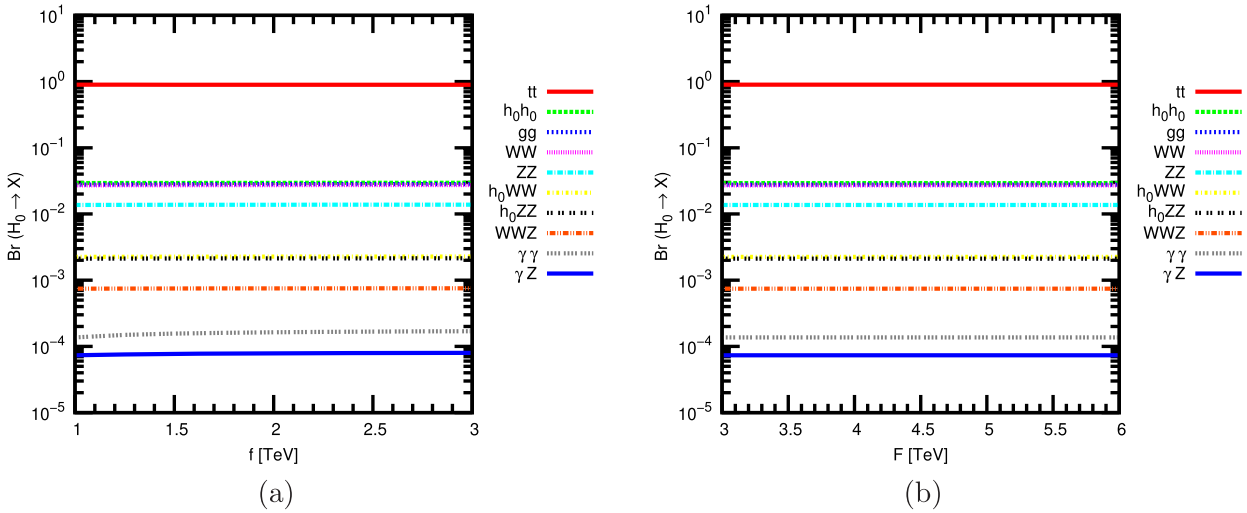

FIG. 5. Branching ratios for the $H_0 \to X$ processes where $X = tt, h_0h_0, gg, WW, ZZ, h_0WW, h_0ZZ, WWZ, \gamma\gamma, \gamma Z$. (a) $\mathrm{Br}(H_0 \to X)$ as a function of the f energy scale (with the fixed value of $F = 4000$ GeV). (b) $\mathrm{Br}(H_0 \to X)$ as a function of the F energy scale (with the fixed value of $f = 1000$ GeV).

that the most suppressed contribution is generated by the $H_0 \to \gamma Z$ decay whose numerical magnitude of its branching ratio is 10^{-5}. The remaining branching ratios turn out to be $\mathrm{Br}(H_0 \to h_0 h_0) \sim \mathrm{Br}(H_0 \to gg) \sim \mathrm{Br}(H_0 \to WW) \sim \mathrm{Br}(H_0 \to ZZ) \sim 10^{-2}$, $\mathrm{Br}(H_0 \to h_0 WW) \sim \mathrm{Br}(H_0 \to h_0 ZZ) \sim 10^{-3}$, and $\mathrm{Br}(H_0 \to WWZ) \sim \mathrm{Br}(H_0 \to \gamma\gamma) \sim 10^{-4}$ for $f = [1000, 3000]$ GeV. In Fig. 5(b) we describe the behavior of $\mathrm{Br}(H_0 \to X)$ when the energy scale F takes values within the set analysis interval. As can be appreciated in the corresponding plot, the dominant branching ratios correspond to the tree-level decays $(H_0 \to \bar{t}t, h_0 h_0)$ of the H_0 Higgs, while the minor contributions arise for one-loop decays $(H_0 \to \gamma\gamma, \gamma Z)$: $\mathrm{Br}(H_0 \to \bar{t}t) = 8.97 \times 10^{-1}$, $\mathrm{Br}(H_0 \to h_0 h_0) = 2.92 \times 10^{-2}$, $\mathrm{Br}(H_0 \to \gamma\gamma) = 1.36 \times 10^{-4}$, and $\mathrm{Br}(H_0 \to \gamma Z) = 7.33 \times 10^{-5}$. For these cases, the numerical predictions of $\mathrm{Br}(H_0 \to X)$ produce constant values over the whole range of F analysis, which also happens for the rest of the H_0 decays, specifically $H_0 \to gg, WW, ZZ, h_0 WW, h_0 ZZ, WWZ$, which generate the following branching ratios: $\mathrm{Br}(H_0 \to gg) = 2.78 \times 10^{-2}$, $\mathrm{Br}(H_0 \to WW) = 2.71 \times 10^{-2}$, $\mathrm{Br}(H_0 \to ZZ) = 1.37 \times 10^{-2}$, $\mathrm{Br}(H_0 \to h_0 WW) = 2.25 \times 10^{-3}$, $\mathrm{Br}(H_0 \to h_0 ZZ) = 2.12 \times 10^{-3}$, and $\mathrm{Br}(H_0 \to WWZ) = 7.45 \times 10^{-4}$. From Figs. 5(a) and 5(b), we find that as f takes values closer to 3000 GeV, the magnitudes of the branching ratios are slightly larger. Complementarily, in Appendix B we provide some values of $\mathrm{Br}(H_0 \to X)$ versus the followings fixed values of $f = 1000$, 2000, 3000 GeV and $F = 3000$ GeV. Thereby, $\mathrm{Br}(H_0 \to X)$ is sensitive to variations in the energy scale f. The above effect does not happen when we vary $\mathrm{Br}(H_0 \to X)$ versus the F scale; this is because, in the study scenario of our choice, the condition $c_g = s_g$ removes dependence on the F scale from (most of) the interaction vertices.

B. Higgs boson production H_0 of the BLHM at the LHC

We present an approximate study of the production cross section of the H_0 Higgs in the BLHM, which has the decay channels $\gamma\gamma$, γZ, and gg. For this purpose, we employ the Breit-Wigner resonant cross section [27]. In this approximation, the production cross section via gluon fusion can be calculated as follows:

$$\sigma(gg \to H_0 \to Y) = \frac{\pi}{36} \frac{\mathrm{Br}(H_0 \to gg)\mathrm{Br}(H_0 \to Y)}{m_{H_0}^2}, \quad (101)$$

where $Y = \gamma\gamma, \gamma Z, gg$. The cross section $\sigma(gg \to H_0 \to Y)$ is determined just at the resonance of the H_0 Higgs. Although the method of analysis proposed in this subsection approximates the production mechanism of a massive scalar particle via gluon fusion, it could provide experimental guidance for the search for new heavy particles of the TeV order.

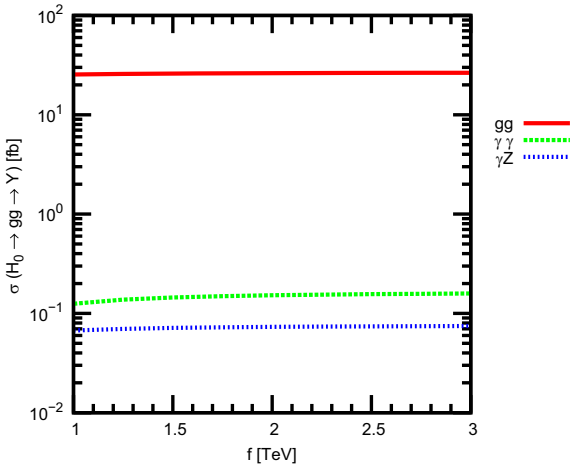

FIG. 6. Production cross section of the H_0 Higgs via gluon fusion as a function of the energy scale f (with the fixed value of $F = 4000$ GeV).

Based on previous studies where the sensitivity of the H_0 partial decay widths and branching ratios on the F energy scale has been analyzed, the numerical estimates suggest that both $\Gamma(H_0 \to X)$ and $\mathrm{Br}(H_0 \to X)$ show almost negligible sensitivity to the F energy scale. Thereby, we compute the H_0 production cross section only as a function of the parameter f, as shown in Fig. 6. In this figure, we observe that the curve providing the largest contribution is generated by the production cross section of H_0 with gg final states, $\sigma(gg \to H_0 \to gg) = [25.45, 26.48]$ fb when $f = [1000, 3000]$ GeV. On the other hand, the weakest contributions arise for $\sigma(gg \to H_0 \to \gamma\gamma) = [1.25, 1.59] \times 10^{-1}$ fb and $\sigma(gg \to H_0 \to \gamma Z) = [6.72, 7.46] \times 10^{-2}$ fb (see the corresponding table in Appendix B for more details). Additionally, we discuss the behavior of $\sigma(gg \to H_0 \to Y)$ versus m_{H_0}, as can be seen in Fig. 7. For the energy scale f, we assign fixed values such as 1000 and 2000 GeV. With these input values for f, we generate the curves shown in Figs. 7(a) and 7(b). Based on the corresponding figures and the numerical estimations, we obtain that the dominant contribution to $\sigma(gg \to H_0 \to Y)$ is reached through the $H_0 \to gg$ decay channel when $f = 1000$ GeV, its production cross section is $\sigma(gg \to H_0 \to gg) = [26.73, 1.68 \times 10^{-1}]$ fb for $m_{H_0} = [1000, 3000]$ GeV. The subdominant contribution emerges when $f = 2000$ GeV, being $\sigma(gg \to H_0 \to gg) = [26.61, 3.08 \times 10^{-1}]$ fb. The other curves generate slightly more suppressed contributions than the main contribution: $\sigma(gg \to H_0 \to \gamma\gamma) = [1.29 \times 10^{-1}, 2.21 \times 10^{-2}]$ fb and $\sigma(gg \to H_0 \to \gamma Z) = [7.15 \times 10^{-2}, 7.14 \times 10^{-3}]$ fb when $f = 1000$ GeV, and $\sigma(gg \to H_0 \to \gamma\gamma) = [1.57 \times 10^{-1}, 3.04 \times 10^{-2}]$ fb and $\sigma(gg \to H_0 \to \gamma Z) = [7.75 \times 10^{-2}, 1.02 \times 10^{-2}]$ fb when $f = 2000$ GeV.

In the experimental scenario, heavy Higgs production mechanisms such as the H_0 Higgs of the BLHM could be

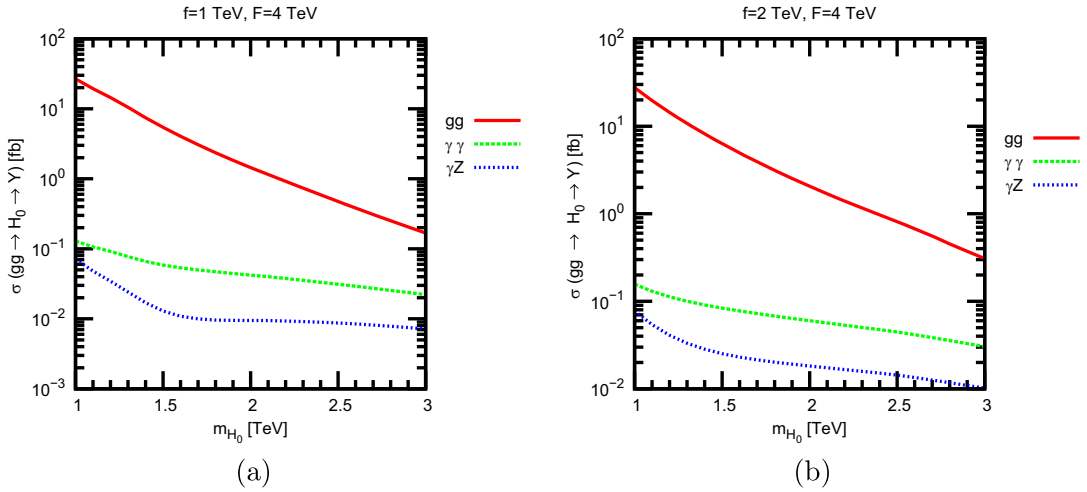

FIG. 7. Production cross section of the H_0 Higgs via gluon fusion as a function of m_{H_0} with (a) $f = 1$ TeV and (b) $f = 2$ TeV.

studied in the context of the LHC and its upgrades [High Luminosity (HL)-LHC and High Energy (HE)-LHC]. After LHC Long Shutdown 2, the expected integrated luminosity of the LHC in Run 3 is approximately 450 fb^{-1} [34]. On the other hand, the HL-LHC [35–37] is planned to operate at a center-of-mass energy of 14 TeV with an integrated luminosity of 3 000 fb^{-1}, while the HE-LHC [35–37] would provide pp collisions with a center-of-mass energy of 27 TeV and an integrated luminosity of 10 000 fb^{-1}. Considering the production cross sections $\sigma(gg \to H_0 \to Y)$ and the expected integrated luminosities of the colliders mentioned above, we can obtain an estimate of the number of events that could be observed at the colliders for the processes of interest. For the purpose of generating a benchmark, considering $m_{H_0} \approx 1000$ GeV, we provide in Tables III,IV,V the expected events related to $H_0 \to gg, \gamma\gamma, \gamma Z$ decays when the scale of the new physics f takes specific values such as 1000, 2000, and 3000 GeV. According to the numerical data, the one-loop decay channel of the H_0 Higgs corresponding to two gluons would be of great interest for the search for the hypothetical heavy particle, the H_0 Higgs of the BLHM. Concerning the $H_0 \to \gamma\gamma, \gamma Z$ decays, their respective expected event magnitudes also promise a very optimistic scenario as they appear to be within the measurement range of the previously proposed future colliders.

TABLE III. Number of expected events related to $H_0 \to gg$ decay.

	No. of expected events at the colliders		
f [TeV]	LHC $\mathcal{L} = 450$ fb^{-1}	HL-LHC $\mathcal{L} = 3000$ fb^{-1}	HE-LHC $\mathcal{L} = 10000$ fb^{-1}
1	11 453	76 355	254 516
2	11 809	78 731	262 438
3	11 914	79 431	264 769

TABLE IV. Number of expected events related to $H_0 \to \gamma\gamma$ decay.

	No. of expected events at the colliders		
f [TeV]	LHC $\mathcal{L} = 450$ fb^{-1}	HL-LHC $\mathcal{L} = 3000$ fb^{-1}	HE-LHC $\mathcal{L} = 10000$ fb^{-1}
1	56	376	1252
2	68	457	1523
3	71	476	1587

TABLE V. Number of expected events related to $H_0 \to \gamma Z$ decay.

	No. of expected events at the colliders		
f [TeV]	LHC $\mathcal{L} = 450$ fb^{-1}	HL-LHC $\mathcal{L} = 3000$ fb^{-1}	HE-LHC $\mathcal{L} = 10000$ fb^{-1}
1	30	202	672
2	33	220	732
3	34	224	746

V. CONCLUSIONS

In this work, we performed a phenomenological study of the production of the heavy Higgs boson H_0 via gluon fusion in the context of the BLHM. Specifically, we analyzed the one-loop decays of the H_0 Higgs, which refer to $H_0 \to gg, \gamma\gamma, \gamma Z$ processes. For these decays, the effects induced by the new particles of the BLHM and the particles of the SM were considered. As the BLHM has two independent energy scales, f and F, these represent the scales of the new physics of the model. In this way, we generated phenomenological results for the branching ratios and production cross sections of the H_0 Higgs in

analysis regions corresponding to $f = [1000, 3000]$ GeV and $F = [3000, 6000]$ GeV. For the considered intervals of the scales f and F, we analyzed the dependence of $\mathrm{Br}(H_0 \to X)$ on the aforementioned scales and found that the branching ratio shows sensitivity to variations in the f scale; this effect is not observed with the F scale. In the two study scenarios, the dominant branching ratios at the tree and one-loop levels correspond to processes $H_0 \to \bar{t}t$ and $H_0 \to gg$ whose numerical predictions are of 10^{-1} and 10^{-2}, respectively. A rough estimate of the production cross section of H_0 was also implemented via gluon fusion. For this case, the numerical estimates of $\sigma(gg \to H_0 \to Y)$ tell us that the $H_0 \to gg$ process offers a very promising scenario for the search for the heavy particle H_0 in future experiments such as the LHC, HL-LHC, and HE-LHC. In this approach, we have that for $m_{H_0} \approx 1000$ GeV and $f = 1$ TeV we could estimate around 11453 events at the LHC, 76 355 events at the HL-LHC, and 254516 events at the HE-LHC, which is a very optimistic scenario for the study of the scalar H_0 predicted by the BLHM.

ACKNOWLEDGMENTS

E. C. A. appreciates the postdoctoral stay at the Universidad Autónoma de Zacatecas. A. G. R. and D. E. G. thank Sistema Nacional de Investigadoras e Investigadores (México).

APPENDIX A: EFFECTIVE COUPLINGS IN THE BLHM

In this appendix, we present the effective couplings involved in our calculation of the production of the heavy Higgs boson H_0.

TABLE VI. Effective couplings involved in our calculation of the production of the H_0 Higgs.

	Effective couplings
$g_{H_0\bar{t}t}$	$\frac{3s_\alpha y_1 y_2 y_3}{(y_1^2+y_2^2)^{1/2}(y_1^2+y_3^2)^{1/2}} - \frac{2s_\alpha s_\beta y_2 y_3 (y_3^2-2y_1^2)v}{f(y_1^2+y_2^2)^{1/2}(y_1^2+y_3^2)}$
$g_{H_0\bar{T}T}$	$-\frac{s_\alpha s_\beta v y_1^2((y_2^2+2y_3^2)y_1^4+(8y_2^2y_3^2-2y_3^4)y_1^2-y_2^2(y_2^4+3y_3^2y_2^2-7y_3^4))}{f(y_1^2+y_2)^{3/2}(y_2^2-y_3^2)(y_1^2+y_3^2)}$
$g_{H_0\overline{T_5}T_5}$	$-\frac{9s_\alpha s_\beta v y_1^2 y_2^2 y_3^3}{f(y_1^2+y_3^2)^{3/2}(y_3^2-y_2^2)}$
$g_{H_0\overline{T_6}T_6}$	$-\frac{c_\alpha c_\beta v y_1}{f}$
$g_{H_0\bar{T}^{2/3}T^{2/3}}$	$-\frac{v y_1(4s_\alpha s_\beta(y_3^2-y_1^2)+c_\alpha c_\beta(y_1^2+y_3^2))}{f(y_1^2+y_3^2)}$
$g_{Z\bar{t}t}$	$-\frac{g}{12c_W}(3c_W^2+s_W^2(4-\frac{y_1^2}{y_1^2+y_2^2})) - \frac{gv^2}{48c_W f^2(y_1^2+y_2^2)^4(y_1^2+y_3^2)^2}(s_\beta^2(3c_W y_3^2(16y_1^{10}+64y_2^2y_1^8+96y_2^4y_1^6+64y_2^6y_1^4-4y_1^4+16y_2^8y_1^2 +4y_2^2y_1^2-y_2^4+16(y_1^2+y_2^2)^4y_3^2)-16s_W^2(y_1^2+y_2^2)^3(4(y2-y3)(y2+y3)y_1^4 -4(y_3^4+2y_2^2y_3^2)y_1^2-3y_2^2y_3^4))-64c_\beta^2 s_W^2 y_2^2(y_1^2+y_2^2)^3(y_1^2+y_3^2)^2)$
$g_{Z\bar{T}T}$	$\frac{g(3c_W^2-s_W^2)}{6c_W} - \frac{2gs_W^2v^2y_1^2(4c_\beta^2(y_2^2-y_3^2)^2+s_\beta^2(2y_2^2+y_3^2)^2)}{3c_W f^2(y_1^2+y_2^2)(y_2^2-y_3^2)^2}$
$g_{Z\bar{T}^{2/3}T^{2/3}}$	$-\frac{g(3c_W^2+7s_W^2)}{6c_W} - \frac{5gs_W^2s_\beta^2v^2}{3c_W f^2}$
$g_{Z\bar{T}_5T_5}$	$-\frac{2gs_W^2}{3c_W} + \frac{3gs_\beta^2v^2y_1^2y_2^2y_3^2(c_W^2(6y_1^2-3y_2^2+9y_3^2)-s_W^2y_3^2)}{4c_W f^2(y_2^2-y_3^2)^2(y_1^2+y_3^2)^2}$
$g_{Z\bar{T}_6T_6}$	$-\frac{2gs_W^2}{3c_W} + \frac{5c_W c_\beta^2 gv^2}{4f^2}$

TABLE VII. Continuation of Table VI.

$g_{\gamma\bar{T}T}$	$\frac{2}{3}gs_W + \frac{gs_Wv^2}{3f^2}(c_\beta^2+s_\beta^2(y_2^2-2y_1^2)^2y_3^2+y_1^2(4c_\beta(y_2^2-y_3^2)^2+s_\beta^2(2y_2^2-y_3^2)^2)$
$g_{\gamma\bar{T}_5T_5}$	$\frac{2}{3}gs_W + \frac{3}{4}gs_W\left(\frac{s_\beta^2v^2y_1^2y_2^2y_3^2(6y_1^2-3y_2^2+10y_3^2)}{f^2(y_2^2-y_3^2)^2(y_1^2+y_3^2)^2}\right)$
$g_{\gamma\bar{T}_6T_6}$	$\frac{2}{3}gs_W + \frac{5gs_Wc_\beta^2v^2}{4f^2}$
$g_{\gamma\bar{T}^{2/3}T^{2/3}}$	$\frac{2}{3}gs_W + \frac{5gs_Ws_\beta^2v^2}{3f^2}$

(Table continued)

TABLE VII. *(Continued)*

$g_{W'W'Z}$	$gc_W - \frac{gv^2x_s(2c_g^2-2s_g^2-c_gs_gc_W(2c_W+1))}{2c_gs_g(f^2+F^2)}$
$g_{W'W'A}$	$gs_W - \frac{gv^2c_Ws_Wx_s}{(f^2+F^2)}$
$g_{WWZ'}$	$\frac{gc_Wv^2x_s}{f^2+F^2}$
g_{WWA}	$gs_W - \frac{g^2c_Ws_Wv^2x_s}{(f^2+F^2)}$
g_{WWZ}	$gc_W - \frac{g^2c_Wv^2x_s(2c_W+1)}{2(f^2+F^2)}$
$g_{h_0ZZ'}$	$-\frac{gs_Wv(c_g^2-s_g^2)(g^2+g'^2)\sin(\alpha+\beta)}{2c_gs_gg'} + \frac{gs_Wv^3(c_g^2-s_g^2)(g^2+g'^2)\sin(\alpha+\beta)}{6c_gs_gg'f^2} + \frac{v^3x_s\sin(\alpha+\beta)(c_g^2gg's_W(g^2+g'^2)+2c_gs_g(g^4s_W^2+g^2g'^2(2s_W^2+1)+g'^4s_W^2)-gg's_g^2s_W(g^2+g'^2))}{2c_gs_gg'^2(f^2+F^2)}$
g_{h_0ZZ}	$\frac{gm_W\sin(\alpha+\beta)}{c_W^2} - \frac{s_W^2v^3(g^2+g'^2)\sin(\alpha+\beta)}{6g'^2f^2} - \frac{s_Wv^3x_s(g^2+g'^2)\sin(\alpha+\beta)(-c_g^2gg'+c_gs_gs_W(g^2+g'^2)+gg's_g^2)}{2c_gs_gg'^2(f^2+F^2)}$
g_{H_0ZZ}	$\frac{s_W^2v(g^2+g'^2)^2\cos(\alpha+\beta)}{2g'^2} - \frac{s_W^2v^3(g^2+g'^2)^2\cos(\alpha+\beta)}{6g'^2f^2} - \frac{s_Wv^3x_s(g^2+g'^2)\cos(\alpha+\beta)(c_g^2(-g)g'+c_gs_gs_W(g^2+g'^2)+gg's_g^2)}{2c_gs_gg'^2(f^2+F^2)}$
$g_{H_0ZZ'}$	$-\frac{gs_Wv(c_g^2-s_g^2)(g^2+g'^2)\cos(\alpha+\beta)}{2c_gs_gg'} + \frac{gs_Wv^3(c_g^2-s_g^2)(g^2+g'^2)\cos(\alpha+\beta)}{6c_gs_gg'f^2} + \frac{v^3x_s\cos(\alpha+\beta)(c_g^2gg's_W(g^2+g'^2)+2c_gs_g(g^4s_W^2+g^2g'^2(2s_W^2+1)+g'^4s_W^2)-gg's_g^2s_W(g^2+g'^2))}{2c_gs_gg'^2(f^2+F^2)}$
g_{H_0WW}	$\frac{1}{2}g^2v\cos(\alpha+\beta) - \frac{g^2v^3\cos(\alpha+\beta)}{6f^2} + \frac{g^3s_Wv^3x_s(c_g^2-c_gs_g-s_g^2)\cos(\alpha+\beta)}{2c_gs_gg'(f^2+F^2)}$
$g_{H_0WW'}$	$-\frac{g^2v(c_g^2-s_g^2)\cos(\alpha+\beta)}{2c_gs_g} + \frac{g^2v^3(c_g^2-s_g^2)\cos(\alpha+\beta)}{6c_gs_gf^2} + \frac{g^3s_Wv^3x_s(c_g^2+4c_gs_g-s_g^2)\cos(\alpha+\beta)}{2c_gs_gg'(f^2+F^2)}$
$g_{H_0W'W'}$	$-\frac{1}{2}g^2v\cos(\alpha+\beta) - \frac{g^2v^3(c_g^4+s_g^4)\cos(\alpha+\beta)}{12c_g^2s_g^2f^2} - \frac{g^3s_Wv^3x_s(c_g^2-c_gs_g-s_g^2)\cos(\alpha+\beta)}{2c_gs_gg'(f^2+F^2)}$
g_{h_0WW}	$gm_W\sin(\alpha+\beta) - \frac{4m_W^2\sin(\alpha+\beta)}{3gf^2} + \frac{4m_W^3s_Wx_s(c_g^2-c_gs_g-s_g^2)\sin(\alpha+\beta)}{c_gs_gg'(f^2+F^2)}$
$g_{h_0WW'}$	$-\frac{g^2v(c_g^2-s_g^2)\sin(\alpha+\beta)}{2c_gs_g} + \frac{g^2v^3(c_g^2-s_g^2)\sin(\alpha+\beta)}{6c_gs_gf^2} + \frac{g^3s_Wv^3x_s(c_g^2+4c_gs_g-s_g^2)\sin(\alpha+\beta)}{2c_gs_gg'(f^2+F^2)}$
$g_{H_0h_0h_0}$	$\frac{1}{4}v\lambda_0(3\cos(3\alpha-\beta)+\cos(\alpha+\beta))$

APPENDIX B: NUMERICAL VALUES FOR $\Gamma(H_0 \to X)$, $\mathrm{Br}(H_0 \to X)$, AND $\sigma(gg \to H_0 \to Y)$

In this appendix, we provide the numerical values of the partial decay widths, branching ratios, and production cross sections of the Higgs boson H_0 when the scales f and F take certain fixed values.

TABLE VIII. Numerical values of the partial decay width of the Higgs boson H_0, corresponding to Fig. 4. Columns 2–4 of this table show the numerical changes of $\Gamma(H_0 \to X)$ vs. f (for $F = 4000$ GeV), while column 5 of $\Gamma(H_0 \to X)$ vs. F (for $f = 1000$ GeV).

	$\Gamma(H_0 \to X)$ [GeV]			
	$F = 4000$ GeV			$f = 1000$ GeV
X	$f = 1$ TeV	$f = 2$ TeV	$f = 3$ TeV	$F = 3$ TeV
tt	4.89×10^{0}	4.84×10^{0}	4.82×10^{0}	4.88×10^{0}
h_0h_0	1.59×10^{-1}	1.59×10^{-1}	1.59×10^{-1}	1.59×10^{-1}
gg	1.51×10^{-1}	1.52×10^{-1}	1.52×10^{-1}	1.51×10^{-1}
WW	1.47×10^{-1}	1.47×10^{-1}	1.47×10^{-1}	1.47×10^{-1}
ZZ	7.45×10^{-2}	7.45×10^{-2}	7.45×10^{-2}	7.45×10^{-2}
h_0WW	1.22×10^{-2}	1.22×10^{-2}	1.22×10^{-2}	1.22×10^{-2}
h_0ZZ	1.15×10^{-2}	1.15×10^{-2}	1.15×10^{-2}	1.15×10^{-2}
WWZ	4.06×10^{-3}	4.06×10^{-3}	4.06×10^{-3}	4.06×10^{-3}
$\gamma\gamma$	7.44×10^{-4}	8.83×10^{-4}	9.14×10^{-4}	7.44×10^{-4}
γZ	4.00×10^{-4}	4.24×10^{-4}	4.30×10^{-4}	3.99×10^{-4}

TABLE IX. Numerical values of the branching ratio of the Higgs boson H_0, corresponding to Fig. 5.

	$\mathrm{Br}(H_0 \to X)$			
	$F = 4000$ GeV			$f = 1000$ GeV
X	$f = 1$ TeV	$f = 2$ TeV	$f = 3$ TeV	$F = 3$ TeV
tt	8.97×10^{-1}	8.96×10^{-1}	8.95×10^{-1}	8.97×10^{-1}
h_0h_0	2.92×10^{-2}	2.95×10^{-2}	2.96×10^{-2}	2.92×10^{-2}
gg	2.78×10^{-2}	2.82×10^{-2}	2.83×10^{-2}	2.78×10^{-2}
WW	2.71×10^{-2}	2.73×10^{-2}	2.74×10^{-2}	2.71×10^{-2}
ZZ	1.37×10^{-2}	1.38×10^{-2}	1.38×10^{-2}	1.37×10^{-2}
h_0WW	2.25×10^{-3}	2.27×10^{-3}	2.28×10^{-3}	2.25×10^{-3}
h_0ZZ	2.12×10^{-3}	2.13×10^{-3}	2.14×10^{-3}	2.12×10^{-3}
WWZ	7.45×10^{-4}	7.52×10^{-4}	7.54×10^{-4}	7.45×10^{-4}
$\gamma\gamma$	1.36×10^{-4}	1.63×10^{-4}	1.70×10^{-4}	1.36×10^{-4}
γZ	7.33×10^{-5}	7.86×10^{-5}	7.98×10^{-5}	7.33×10^{-5}

TABLE X. Numerical values of the production cross section of the Higgs boson H_0 via gluon fusion, corresponding to Fig. 6.

	$\sigma(gg \to H_0 \to Y)$ [fb]		
	$F = 4000$ GeV		
Y	$f = 1$ TeV	$f = 2$ TeV	$f = 3$ TeV
gg	25.45×10^{0}	26.24×10^{0}	26.48×10^{0}
$\gamma\gamma$	1.25×10^{-1}	1.52×10^{-1}	1.59×10^{-1}
γZ	6.72×10^{-2}	7.32×10^{-2}	7.46×10^{-2}

[1] M. Schmaltz, D. Stolarski, and J. Thaler, J. High Energy Phys. 09 (2010) 018.
[2] S. Godfrey, T. Gregoire, P. Kalyniak, T. A. W. Martin, and K. Moats, J. High Energy Phys. 04 (2012) 032.
[3] P. Kalyniak, T. Martin, and K. Moats, Phys. Rev. D **91**, 013010 (2015).
[4] T. Cisneros-Pérez, M. A. Hernández-Ruíz, A. Gutiérrez-Rodríguez, and E. Cruz-Albaro, Eur. Phys. J. C **83**, 1093 (2023).
[5] E. Cruz-Albaro, A. Gutierrez-Rodrıguez, M. A. Hernandez-Ruız, and T. Cisneros-Perez, Eur. Phys. J. Plus **138**, 506 (2023).
[6] E. Cruz-Albaro, A. Gutiérrez-Rodríguez, J. I. Aranda, and F. Ramírez-Zavaleta, Eur. Phys. J. C **82**, 1095 (2022).
[7] E. Cruz-Albaro and A. Gutiérrez-Rodríguez, Eur. Phys. J. Plus **137**, 1295 (2022).
[8] N. Arkani-Hamed, A. G. Cohen, E. Katz, and A. E. Nelson, J. High Energy Phys. 07 (2002) 034.
[9] S. Chang, J. High Energy Phys. 12 (2003) 057.
[10] T. Han, H. E. Logan, B. McElrath, and L. T. Wang, Phys. Rev. D **67**, 095004 (2003).
[11] S. Chang and J. G. Wacker, Phys. Rev. D **69**, 035002 (2004).
[12] M. Schmaltz, J. High Energy Phys. 08 (2004) 056.
[13] M. Schmaltz and J. Thaler, J. High Energy Phys. 03 (2009) 137.
[14] X. F. Han, L. Wang, J. M. Yang, and J. Zhu, Phys. Rev. D **87**, 055004 (2013).
[15] J. Reuter and M. Tonini, J. High Energy Phys. 02 (2013) 077.
[16] C. Csaki, J. Hubisz, G. D. Kribs, P. Meade, and J. Terning, Phys. Rev. D **67**, 115002 (2003).
[17] ATLAS Collaboration, Combined measurements of Higgs boson production and decay using up to 80 fb^{-1} of proton-proton collision data at $\sqrt{s} = 13$ TeV collected with the ATLAS experiment, ATLAS-CONF-2019-005.
[18] K. P. Moats, Phenomenology of Little Higgs models at the Large Hadron Collider (2012), 10.22215/etd/2012-09748.
[19] D. Eriksson, J. Rathsman, and O. Stal, Comput. Phys. Commun. **181**, 189 (2010).
[20] T. A. W. Martin, Examining extra neutral gauge bosons in non-universal models and exploring the phenomenology of the Bestest Little Higgs model at the LHC (2012), 10.22215/etd/2012-09697.
[21] S. P. Martin, Adv. Ser. Dir. High Energy Phys. **18**, 1 (1998).
[22] G. Aad *et al.* (ATLAS Collaboration), Phys. Lett. B **809**, 135754 (2020).

[23] A. Tumasyan *et al.* (CMS Collaboration), J. High Energy Phys. 05 (2023) 233.
[24] A. M. Sirunyan *et al.* (CMS Collaboration), Phys. Lett. B **805**, 135425 (2020).
[25] A. Gutiérrez-Rodríguez, E. Cruz-Albaro, and D. Espinosa-Gómez, arXiv:2312.08560.
[26] J. I. Aranda, T. Cisneros-Pérez, E. Cruz-Albaro, J. Montaño-Domínguez, and F. Ramírez-Zavaleta, arXiv:2111.03180.
[27] R. L. Workman *et al.* (Particle Data Group), Prog. Theor. Exp. Phys. **2022**, 083C01 (2022).
[28] E. Barradas, J. L. Diaz-Cruz, A. Gutierrez, and A. Rosado, Phys. Rev. D **53**, 1678 (1996).
[29] A. Denner and S. Dittmaier, Nucl. Phys. **B734**, 62 (2006).
[30] W. Altmannshofer and D. M. Straub, J. High Energy Phys. 09 (2010) 078.
[31] R. L. Workman *et al.* (Particle Data Group), Prog. Theor. Exp. Phys. **2022**, 083C01 (2022).
[32] G. Aad *et al.* (ATLAS Collaboration), Eur. Phys. J. C **81**, 396 (2021).
[33] A. M. Sirunyan *et al.* (CMS Collaboration), J. High Energy Phys. 03 (2020) 055.
[34] CERN, 2022, https://hilumilhc.web.cern.ch/article/ls3-schedule-change.
[35] A. Abada *et al.* (FCC Collaboration), Eur. Phys. J. Special Topics **228**, 1109 (2019).
[36] A. Abada *et al.* (FCC Collaboration), Eur. Phys. J. C **79**, 474 (2019).
[37] A. Abada *et al.* (FCC Collaboration), Eur. Phys. J. Special Topics **228**, 755 (2019).